Autonomous Navigation in Lunar Lava Tubes: Sensing SLAM Trade-Offs and a Mission-Oriented GNC Architecture

robotics

MDPI

Article

Autonomous Navigation in Lunar Lava Tubes: Sensing SLAM Trade-Offs and a Mission-Oriented GNC Architecture

Giulia Calvo [1,*], Alessandro Cimini [1], Matteo Melchiorre [1], Laura Salamina [1], Cuono Massimo Crispo [2], Francesco Saverio Fulginiti [2], Isacco Pretto [2], Tharek Mohtar [2] and Stefano Mauro [1]

[1] Department of Mechanical and Aerospace Engineering, Politecnico di Torino, Corso Duca degli Abruzzi 24, 10129 Torino, TO, Italy; alessandro.cimini@polito.it (A.C.); matteo.melchiorre@polito.it (M.M.); laura.salamina@polito.it (L.S.); stefano.mauro@polito.it (S.M.)

[2] OHB Italia SpA, Via Gallarate, 150, 20151 Milano, MI, Italy; massimo.crispo@ohb-italia.it (C.M.C.); francescosaverio.fulginiti@ohb-italia.it (F.S.F.); isacco.pretto@ohb-italia.it (I.P.); tharek.mohtar@ohb-italia.it (T.M.)

* Correspondence: giulia.calvo@polito.it

Abstract

Lunar lava tubes are subsurface cavities generated by volcanic activity and are regarded as promising targets for exploration because they can offer natural shielding and potentially support future lunar infrastructures as protected shelters and scientific laboratories. Autonomous navigation in these environments remains challenging due to the absence of illumination, sparse or repetitive geometric features, uneven terrain, and intermittent communications that limit teleoperation. In this framework, the Italian Space Agency (ASI) is pursuing a dedicated mission, and OHB Italia has been appointed the prime contractor to perform a candidate system-architecture study for lava tube exploration. This paper presents the activities and results related to the definition of the subsurface Guidance, Navigation, and Control (GNC) algorithm for a rover/hopper system. To address the above constraints, this study investigates the requirements for autonomous onboard navigation, focusing on sensor selection for Simultaneous Localization and Mapping (SLAM) as a fundamental prerequisite for mission success. A weighted-criteria evaluation framework is developed to assess various sensing modalities, considering mission-specific constraints. Based on this analysis, a sensor configuration optimized for GPS-denied and unilluminated environments is proposed. The effectiveness of the selected sensing architecture is validated through a simulation campaign conducted in simulation environments (CoppeliaSim v4.10.0/MATLAB 2025a), using two representative SLAM pipelines (ICP and LOAM) in LiDAR-only and LiDAR + IMU configurations. Finally, a modular Guidance, Navigation, and Control (GNC) architecture incorporating frontier-based exploration is proposed.

Keywords: autonomous navigation; lunar lava tubes exploration; SLAM

Academic Editors: Jinjin Yan and Minzhou Luo

Received: 4 April 2026
Revised: 21 May 2026
Accepted: 25 May 2026
Published: 29 May 2026

1. Introduction

In the context of robotic exploration of the Solar System, the Moon is considered a target of greatest interest, as it is the first and most accessible destination beyond low Earth orbit (LEO) and as an intermediate step for future initiatives aimed at Mars [1].

The Moon has emerged as a focal point and frontier for deep space exploration, ushering in a new era where both scientific investigation and space utilization are of equal significance [2].

The environments of extraterrestrial bodies are typically harsh, with extreme temperature variations, frequent micrometeorite impacts, and intense cosmic radiation [3,4]. In addition, there is evidence that small particles comprising the lunar regolith can be electrically charged, mobilized, and transported, also representing a hazard for covering sensitive surfaces and interfering with exposed mechanical structures [5]. Therefore, long-term human presence will first require identifying or establishing shelters that are safe, stable, and durable. As a result, subsurface structures are particularly attractive because they can offer natural shielding from these hazards.

Lunar lava tubes are subsurface cavities formed by volcanic processes on planetary bodies [6] and could provide critical shelter for future infrastructure while enabling scientific investigations that are difficult to conduct on the exposed surface.

From the standpoint of exploration, lava tubes present compounded operational hazards: steep slopes at pit funnels, vertical drops, uneven terrain, complete absence of natural illumination, and a partially unknown geometry. Solution based on spherical rovers such as those described in [7,8] could be suitable for operation in this environment. In addition, communications can be intermittent or severely attenuated, which reduces the feasibility of continuous teleoperation and shifts the burden toward onboard autonomy [9]. These constraints imply that, to carry out exploration effectively, lava tube missions require a robotic system that cannot rely on continuous ground supervision and must instead localize and map onboard while planning safe motions toward scientific targets.

Within this context, the Italian Space Agency (ASI) is pursuing the development of a robotic mission to the unexplored lunar surface, aimed at enabling autonomous exploration of the environment inside lunar lava tubes. OHB Italia has been commissioned as the prime contractor to develop a candidate mission architecture, including comparative trade-off analyses at the system level. This work presents the activities and results obtained for the definition of the surface Guidance, Navigation, and Control (GNC) algorithm for a rover/hopper dedicated to lava tube exploration.

Ensuring reliable autonomous operation in such an unfamiliar and challenging environment requires the rover/hopper to provide robust environmental perception, high-precision positioning, and autonomous obstacle avoidance capabilities [10]. In the complex and unknown lunar environment, lunar rover position and map creation should be considered together, which is known as the SLAM (Simultaneous Localization and Mapping) problem. SLAM refers to the robot constructing the surrounding environment map incrementally when moving in an unknown environment, while simultaneously estimating its own pose within that map [11]. The robot state is described by its pose (position and orientation), although other quantities may be included in the state, such as robot velocity, sensor biases, and calibration parameters. The map, on the other hand, is a representation of aspects of interest (e.g., position of landmarks, obstacles) describing the environment in which the robot operates [12]. The knowledge of the position of the obstacles can support collision-avoidance algorithms, such as those described in [13], while a digital twin of the system [14] can improve the capability to track the rover in the absence of communication.

SLAM needs to use the external sensor to digitize the scene first. Although laser, sonar, and other sensors are commonly used on ground robots, their application in planetary subsurface environments is constrained by the complexity of the operating conditions [11]. The choice of sensing modality is therefore decisive, because it directly determines observability, failure modes, computational load, and power demand in a resource-constrained planetary rover. Recent research on SLAM for lunar applications has produced a wide range of solutions based on vision, LiDAR, and their combinations; however, performance is often assessed in scenarios and with metrics that are not fully aligned with the distinctive

constraints of lunar lava tubes (e.g., complete absence of illumination, severe link attenuation, intermittent texture/feature availability, and stringent limitations in power and onboard computation).

Several advanced LiDAR-Inertial SLAM algorithms exist; the present study focuses on the sensor suite selection rather than on the comparison of specific SLAM implementations. ICP and LOAM were selected as representative algorithms to evaluate the incremental benefit of IMU fusion in the target environment.

Motivated by the above, an analysis of sensing options for lava tube navigation is conducted in this work.

Unlike approaches mainly focused on specific robotic systems or external communication strategy, this work addresses sensing and autonomous navigation from a mission-level perspective, combining criteria-based sensor selection, simulation-based validation, and system-level interpretation to support the definition of a navigation architecture under lava tube constraints. The analysis and the simulations carried out to support it are related only to the navigation inside the lava tube, which is expected to extend for several tens of meters in the absence of light. Sensor SLAM configurations are assessed using a weighted-criteria evaluation framework designed to reflect mission-specific operational needs and system-level constraints, with the aim of selecting the most suitable suite of sensors for the specific mission. The resulting selection is then validated by testing existing SLAM algorithms from the literature, namely ICP and LOAM, each tested under two sensing modalities: LiDAR-only and LiDAR + IMU. To generate realistic test data, a lava tube-like environment and rover sensing are modeled in a physics-based simulator (CoppeliaSim v4.10.0) [15]. The resulting LiDAR point clouds and IMU measurements are exported and post-processed in MATLAB to benchmark localization performance and quantify the contribution of IMU information to localization consistency.

Finally, the navigation outcomes are translated into a modular subsurface GNC architecture and an exploration-oriented operational logic consistent with lava tube constraints.

2. Navigation in Lava Tubes: Problem Setting and Constraints

Lava tubes are natural tunnels formed by lava flowing from volcanic vents. During the flow of low-viscosity basaltic lava, the surface cools and solidifies, forming a crust. This crust acts as an insulating layer, reducing the cooling rate of the lava inside. The molten lava within continues to flow at high temperatures for hundreds to thousands of kilometers until the source ceases to supply lava, resulting in a hollow tube known as a lava tube [16].

To date, more than 300 caves have been identified on the lunar surface; however, only 21 are considered potential entrances to underground lava tubes, with 16 located in the mare regions and five in the highland region, as shown in Figure 1.

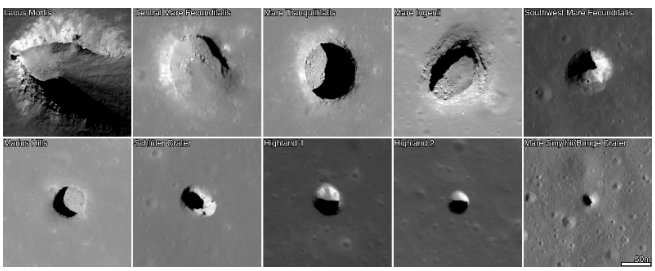

Figure 1. Collection of pits detected on the Moon—source NASA.

Lunar lava tubes are compelling candidates for future exploration infrastructure because they provide strong natural protection from the harsh surface environment [17].

Owing to the absence of both a substantial atmosphere and a global magnetic field, the lunar surface is continuously exposed to Galactic Cosmic Rays (GCRs) and Solar Energetic Particles (SEPs): estimated cosmic-ray doses can reach ~416 mSv/year, while SEP events may deliver doses up to ~2190 mSv per event. In contrast, the radiation dose inside a lunar lava tube is expected to be below ~1 mSv/year, indicating a dramatically safer environment than the exposed surface [18].

In addition to shielding against high-energy particle bombardment, the ceilings of lava tubes, with a shielding thickness on the order of meters to tens of meters, offer protection against micrometeoroid impacts.

Furthermore, their association with volcanic terrains may offer additional in situ resource opportunities, including access to volatile chemical species such as sulfur, iron, and oxygen, together with pyroclastic debris that could be used as construction material [19].

However, the exploration problem is dominated by environmental constraints. Entrances may be vertical or sloped, frequently associated with debris accumulation and irregular, potentially sharp or unstable walls, complicating safe ingress/egress and increasing mobility risk near the pit floor.

Inside the lava tubes, traversability is highly non-uniform due to rubble fields, cracks, and local collapses.

Illumination is effectively absent beyond limited skylight penetration, pushing perception toward active sensing and robust mapping/localization under uncertainty. Communication represents another first-order constraint: rock shielding and curved/uneven propagation paths lead to strong attenuation and multipath fading, often limiting bandwidth and reliability and motivating relay/repeater architectures for sustained operations.

Similar challenges have been addressed in terrestrial subterranean robotics, where autonomous navigation in GPS-denied and visually degraded environments has been extensively studied [20].

Consequently, autonomous exploration in these environments requires robots and operational strategies capable of robust navigation under highly non-uniform traversability, along with a carefully selected active sensing suite to ensure accurate mapping and localization under severe uncertainty.

3. Evaluation Framework: Metrics and Design Criteria

Given the lava tube constraints described in Section 2—absence of natural illumination, limited a priori knowledge of geometry, non-uniform traversability, and the need to operate with bounded onboard resources and potentially intermittent data streams—the SLAM subsystem must be selected through a structured trade-off rather than based on accuracy alone. The purpose of this trade-off study is to identify the most suitable SLAM architecture for supporting autonomous exploration of a lunar lava tube, accounting for mission-specific requirements and the associated technical and programmatic risks.

An evaluation of different SLAM architectures (e.g., Visual, Visual-Inertial, RGB-D, LiDAR-based, and LiDAR-Inertial) is conducted to select the most appropriate configuration for the mission.

Candidate SLAM design solutions were evaluated using a set of criteria selected to reflect mission-specific operational needs and system-level constraints. These criteria capture the key technical factors that influence the performance, feasibility, and reliability of each alternative.

The selected evaluation criteria are as follows:

- Localization accuracy: The ability of the system to reliably estimate the rover's position and orientation over time.

- Robustness to environmental conditions: Resilience to variations in terrain morphology and unknown structures.
- Robustness to data interruptions: The capability to maintain localization performance in case of temporary sensor data loss or degradation.
- Lighting conditions: The system's dependence on the availability of ambient or artificial light for correct operation.
- Data processing speed: The ability to process sensory data in real time to support timely localization and mapping outputs.
- Energy consumption: The impact on the rover's power budget, which is a critical factor for mission duration.
- Hardware complexity: The number and type of sensors required, and their impact on onboard integration and data handling.
- System integration complexity: The effort required to integrate the SLAM system with the overall avionics and onboard software architecture.

In Table 1, each criterion was assigned a weighting factor (a value from 1 to 5) to reflect its relative importance within the mission context.

Table 1. Evaluation criteria for lunar rover navigation and localization systems.

Criterion	Weight	Justification
Localization Accuracy	5	Accurate localization is crucial for the rover to navigate autonomously and effectively. This is the highest priority in ensuring the rover can understand its position accurately in both planned and unknown environments.
Robustness to Environmental Conditions	4	The ability to withstand changing environmental factors, such as terrain variability, is essential but slightly less critical than localization accuracy.
Robustness to Data Interruptions	4	On the lunar surface, data interruptions are less critical because the rover is teleoperated, and the operator can manage interruptions. However, inside lava tubes, where the rover operates autonomously in an unknown and dark environment, data interruptions could lead to severe navigation issues. Therefore, robust handling of data interruptions is crucial in lava tube navigation.
Sensitivity to Lighting Conditions	3	The impact of lighting conditions is important but less critical, as some SLAM algorithms can function in a variety of light conditions, especially when combined with LiDAR or other sensors.
Data Processing Speed	3	The low speed of the rover reduces the need for extremely fast data processing, as the rover has more time to process sensor data. However, real-time processing is strictly required for effective navigation and map construction. Data processing speed is also affected by the complexity of the algorithm.
Energy Consumption	4	Energy consumption of the GNC system (sensors and OBC) can significantly affect the autonomy of the system.
Hardware Complexity	3	The integration of redundant sensors and systems increases the overall hardware complexity. Ensuring mission continuity in case of sensor failure requires sophisticated sensor fusion and data management, which adds significant complexity to the design and integration of the hardware.
System Integration Complexity	4	Integrating redundant sensors (such as multiple LiDAR or IMU) adds significant complexity to the system. This is especially true for the fusion of sensor data, calibration, and synchronization, all of which are critical to ensure reliability in a harsh lunar environment. The increased complexity also supports the need for a robust fault tolerance system, which is essential in such a mission.

4. Analysis Sensor Modalities for Subsurface Planetary Navigation

Following the definition of mission-driven evaluation criteria, the candidate SLAM architectures are analyzed according to how their underlying sensor modalities (camera, IMU, and LiDAR) address the principal lava tube constraints.

Four alternatives are considered: Visual-only SLAM, Visual–Inertial SLAM, LiDAR-only SLAM, and LiDAR–Inertial SLAM.

Visual-only SLAM relies on visual sensors as the main data input for its application, offering cost-effectiveness and rich visual information about the environment [21]. V-SLAM estimates the rover's pose and builds a map from monocular or stereo imagery through feature extraction and temporal tracking. Although widely validated in terrestrial robotics, its applicability in lava tubes is fundamentally limited by the need for reliable illumination and sufficient texture, and it is sensitive to dust-induced occlusion and saturation effects, yielding elevated operational risk despite high maturity in Earth settings.

Visual–Inertial SLAM augments vision with inertial sensors, improving short-term motion observability. Inertial information (i.e., linear acceleration and rotational velocity measured by the IMU sensor) is modeled by inertial navigation and can compensate for the defects of visual information [22]. However, performance remains dependent on accurate calibration and time synchronization, and the approach does not remove the intrinsic dependence on usable imagery in persistently dark segments unless active lighting is carried (with associated power and integration impacts) [23].

LiDAR-only SLAM relies on scan matching and point-cloud registration from active range sensing, offering strong resilience to lighting conditions and generally robust behavior in cluttered, unstructured environments. Compared with the visual SLAM, LiDAR-SLAM can accomplish its own localization and mapping under more diversified environmental conditions [24]. However, its reliability can degrade in locally smooth or repetitive geometry where registration becomes ill-conditioned, and LiDAR payloads typically impose higher mass/power and data-handling demands than camera-based stacks [25].

Finally, LiDAR–Inertial SLAM couples LiDAR registration with inertial propagation, using the IMU to provide a motion prior that improves convergence and robustness under partial occlusion, rapid maneuvers, or transient LiDAR degradation; this combination is typically the most reliable in environments with minimal visual cues, at the cost of increased system complexity and compute/power requirements that must be traded against overall GNC budgets [26,27].

In Table 2, the alternatives are scored against the criteria defined previously, and the total score is then computed using mission-driven weights.

The reported scores are assigned according to a qualitative criteria-based assessment defined by the authors. This assessment accounts for the literature-supported characteristics of the SLAM methods under consideration, as well as the operational constraints identified for lunar lava tube exploration.

Specifically, the scoring of each architecture on criteria such as lighting sensitivity, robustness to environmental conditions, and localization accuracy is based on the performance trends and failure modes documented in [22–29], ensuring that the assigned values reflect the published evidence.

Scores are assigned on a 1–6 scale, where 1 denotes the lowest performance and 6 denotes the highest performance, except where otherwise specified.

The outcome indicates that Visual-only SLAM and Visual–Inertial SLAM are penalized by lighting dependence and reduced robustness under subsurface conditions.

LiDAR-based solutions provide the most favorable balance for subsurface navigation, with LiDAR-only SLAM and especially LiDAR–IMU SLAM achieving the highest aggregate performance; these approaches best satisfy the dominant mission drivers—lighting

independence, robustness to environmental variability, and reliable localization—while keeping resource and integration trade-offs within manageable bounds.

Table 2. SLAM architectures scored for trade-off analysis.

	Weight	Visual—Only SLAM	Visual-Inertial SLAM	LiDAR-Only SLAM	LiDAR + IMU SLAM
Localization accuracy	5	3	4	4	6
Robustness to environmental condition	4	2	3	4	6
Robustness to data interruptions	4	2	4	4	5
Sensitivity to lighting conditions	4	2	2	5	5
Data processing speed	3	4	3	3	2
Energy consumption	3	5	4	4	3
Hardware complexity	3	4	3	4	3
System integration complexity	4	5	4	4	3
TOTAL SCORE		101	104	120	128

To assess the stability of the resulting ranking, a sensitivity analysis was performed by independently perturbing each criterion weight by ± 1 (on the 1–5 scale) while keeping all scores fixed, and by perturbing individual scores by ± 1 while keeping weights fixed.

The ranking remains unchanged under all single-parameter perturbations. For instance, decreasing the LiDAR–Inertial score for the highest-weight criterion (localization accuracy) by 1 reduces its total score from 128 to 123, which remains higher than the LiDAR-only total score (120). Conversely, increasing the LiDAR-only score in the same criterion raises its total score to 125, still below the LiDAR–Inertial total score.

The sensitivity analysis confirms that the preference for the LiDAR–Inertial configuration is robust, with the 8-point margin not being overturned by realistic single-parameter variations. The LiDAR-only solution may therefore be considered a secondary option under specific constraints.

5. MATLAB Simulation and Results

A dedicated simulation campaign was implemented to assess the SLAM architecture selected through the trade-off and to verify its expected behavior in a representative subsurface setting. The reference environment was reproduced in CoppeliaSim, while post-processing and algorithm evaluation were performed in MATLAB.

The purpose of the simulation campaign is to verify the advantage of the chosen sensor configuration (LiDAR + IMU) using two established and computationally different approaches (feature-based vs. registration-based). A comparison between different existing SLAM algorithms is not in the scope of this work.

Sensor datasets consisted of LiDAR point clouds generated from the simulator using a rotating Velodyne VPL-16 model and inertial outputs obtained by combining the accelerometer and gyroscope models, with additional noise injected in MATLAB based on LN-200S specifications, from Northrop Grumman (Falls Church, VA, USA), to emulate drift and achieve more realistic conditions.

In order to build the simulation environment, a search for possible 3D scenes representative of a lava tube was performed. In [28], it is possible to find point clouds of craters and tunnels considered by NASA to be of interest for the study of planetary exploration. Figure 2 shows measurements of parts of these sites, provided as point clouds, and mesh reconstructions made in MATLAB. These meshes, then imported into CoppeliaSim, form the scene in which the rover navigates.

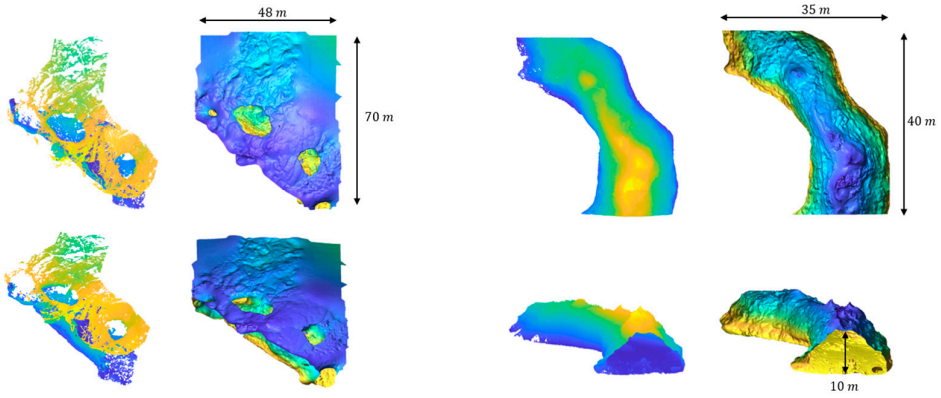

Figure 2. Point clouds of craters and tunnels—source NASA.

In the simulated environment (shown in Figure 3), the rover performs a rectilinear trajectory while the LiDAR sensor acquires point clouds of the surrounding environment and the IMU records angular velocity and acceleration data. These datasets are stored in .csv files and post-processed using MATLAB. The point clouds are reformatted to be compatible with the algorithms, and noise is injected into the IMU data to better simulate the selected sensors.

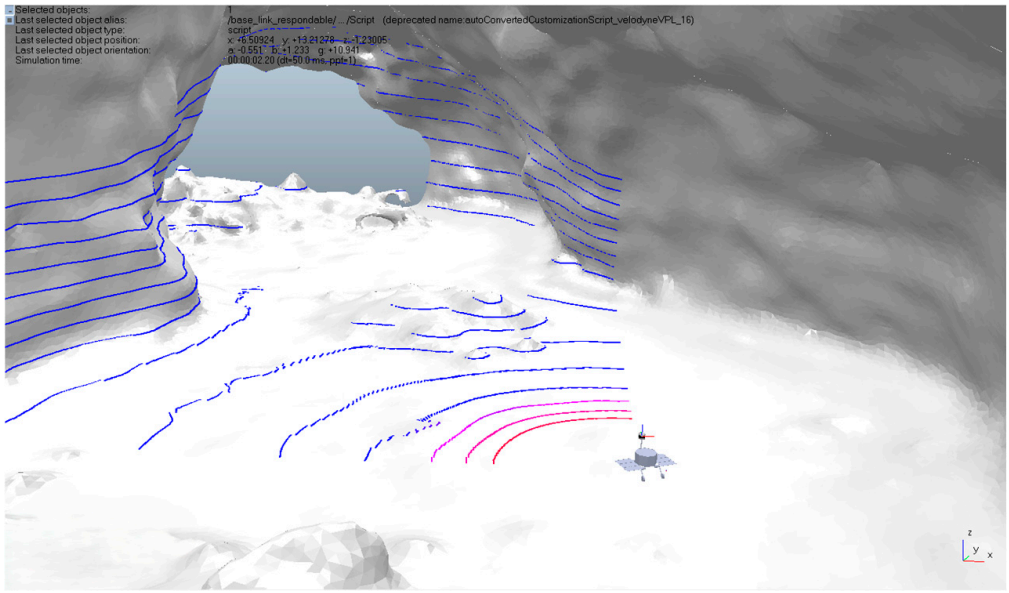

Figure 3. CoppeliaSim setup.

Within this framework, two LiDAR-based SLAM algorithms—ICP and LOAM—were selected as test cases to compare localization performance in two sensing configurations: LiDAR-only and LiDAR-Inertial. The goal is to use the simulation as a controlled benchmark to isolate and quantify the contribution of inertial information to localization consistency, in order to verify the opportunity to adopt the selected architecture even if it increases the complexity in the hardware and requires greater computation capability with respect to simpler solutions.

The LOAM algorithm estimates the sensor motion by extracting distinct geometric features (typically edge-like and planar points) from each LiDAR scan, downsampling them, and aligning the current features to those from the previous scan to compute inter-scan odometry [25]. The resulting pose estimate is subsequently refined through scan-to-map registration against an incrementally constructed global map. When inertial measure-

ments are available, IMU data are used to provide an initial motion prior, improving pose initialization and increasing robustness during the optimization process.

Figure 4 illustrates the reconstructed trajectories in the XY plane. Both the standard LOAM configuration and the LOAM + IMU configuration closely follow the ground-truth trajectory, indicating accurate estimation of planar motion. This behavior can be attributed to the strong geometric constraints typically available in the horizontal plane, where a sufficient spatial distribution of edge and planar features ensures good observability. As a result, the scan-to-scan and scan-to-map alignment processes remain well-conditioned, limiting drift accumulation in the planar components.

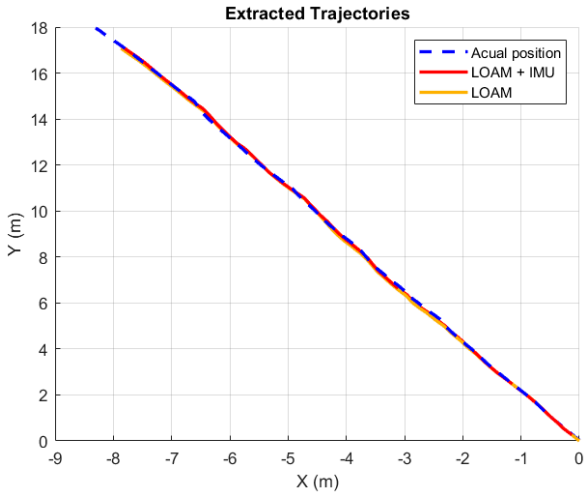

Figure 4. X-Y plane trajectory reconstruction (LOAM).

In contrast, the vertical component, shown in Figure 5, exhibits more pronounced discrepancies for the LiDAR-only solution. Height estimation is inherently more sensitive to terrain morphology and feature distribution. Small alignment errors can therefore accumulate over time, leading to systematic drift in the estimated height. This effect is particularly evident in the standard LOAM results, where the trajectory progressively diverges from the ground-truth profile.

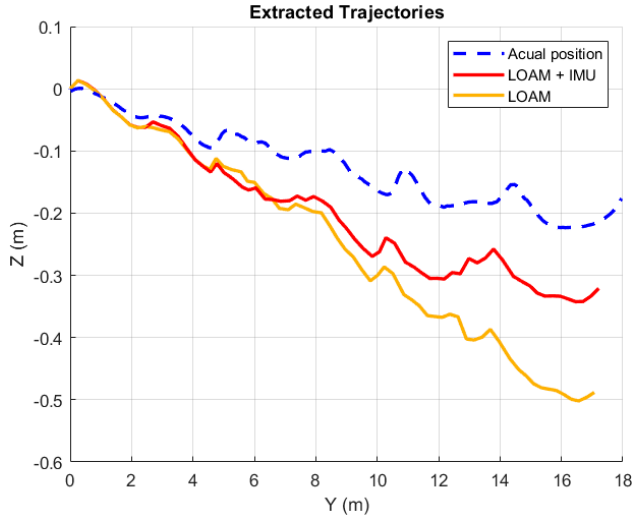

Figure 5. Z-Y plane trajectory reconstruction (LOAM).

The integration of IMU measurements mitigates this issue by introducing complementary constraints. Although pure inertial integration would suffer from long-term drift, its fusion with LiDAR measurements yields a synergistic effect: LiDAR corrections bound

inertial drift over time, while inertial priors enhance convergence and robustness in geometrically weak scenarios. Consequently, the LOAM + IMU configuration exhibits reduced drift in the Z component and improved consistency with the ground-truth height profile.

Overall, the results demonstrate that while LiDAR-only odometry is sufficient for accurate planar reconstruction, multi-sensor fusion significantly enhances robustness in the presence of elevation variability. The inclusion of inertial aiding improves vertical stability, reduces cumulative drift, and increases the overall reliability of the trajectory estimation process.

Despite the height-tracking difficulty, LOAM produces a coherent map with an overall accurate representation of the environment, as shown in Figure 6. A false-color elevation map is used to visualize the surface morphology, with colder colors representing lower regions and warmer colors representing higher regions.

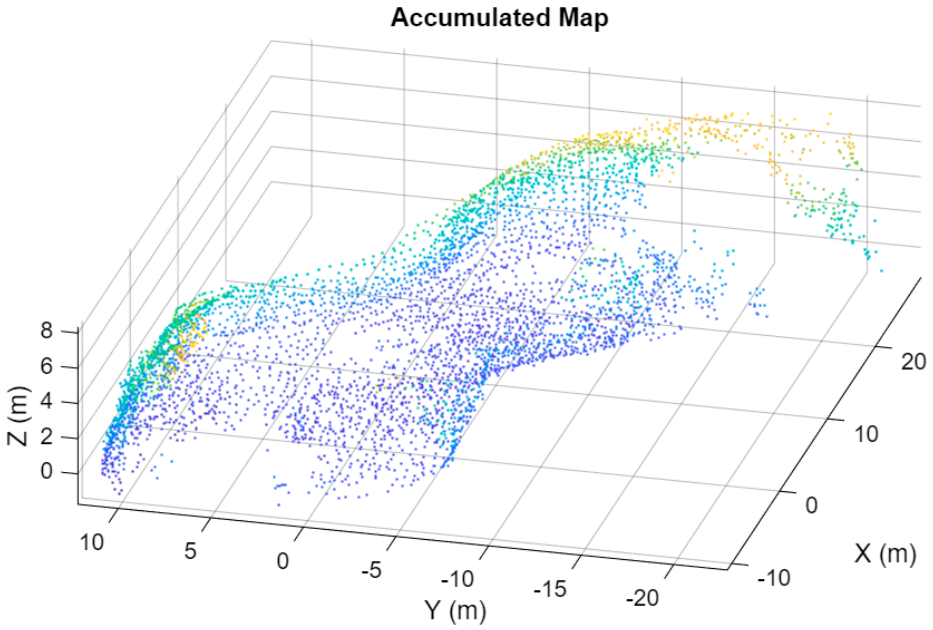

Figure 6. LOAM-generated map.

ICP was implemented as a geometry-based registration pipeline. After voxel-grid downsampling, each LiDAR scan was aligned to the subsequent one by iteratively estimating the rigid transformation that minimizes point-to-point residuals [29] until convergence. The resulting sequence of inter-scan transformations was then composed to recover the absolute trajectory, and the map was built by transforming each scan into the global frame using the accumulated poses. As shown in Figures 7 and 8, ICP provides a closer agreement with the ground-truth trajectory, with a particularly improved behavior on the Z component, and it also yields a more detailed reconstruction (Figure 9). This result is consistent with the characteristics of the lava tube environment, where the low density of salient geometric features (e.g., sharp edges and distinctive planar patches) weakens the constraints exploited by feature-based pipelines such as LOAM. In contrast, ICP directly leverages dense geometric consistency and benefits from the high scan overlap induced by the rover's slow motion and the largely smooth, continuous surfaces, which improve registration conditioning and reduce the probability of incorrect associations.

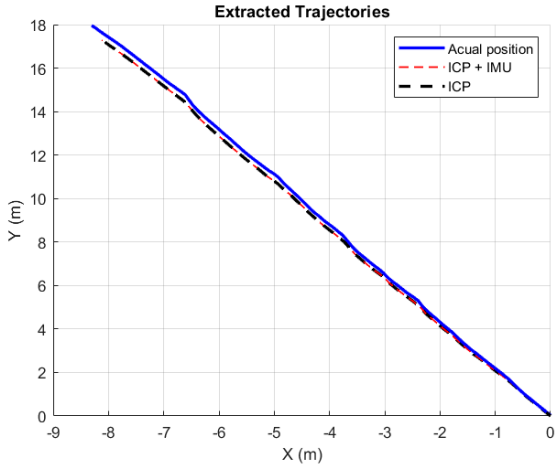

Figure 7. X-Y plane trajectory reconstruction (ICP).

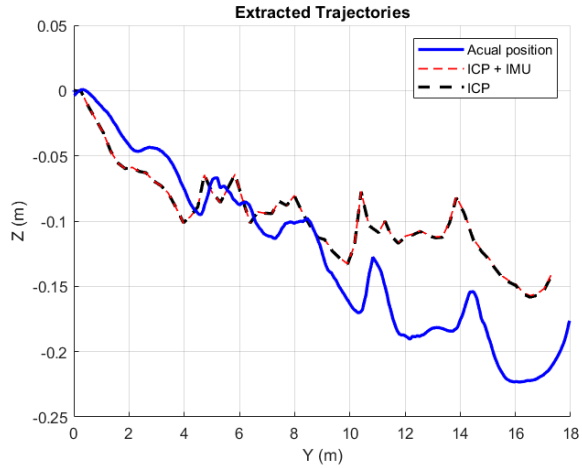

Figure 8. Z-Y plane trajectory reconstruction (ICP).

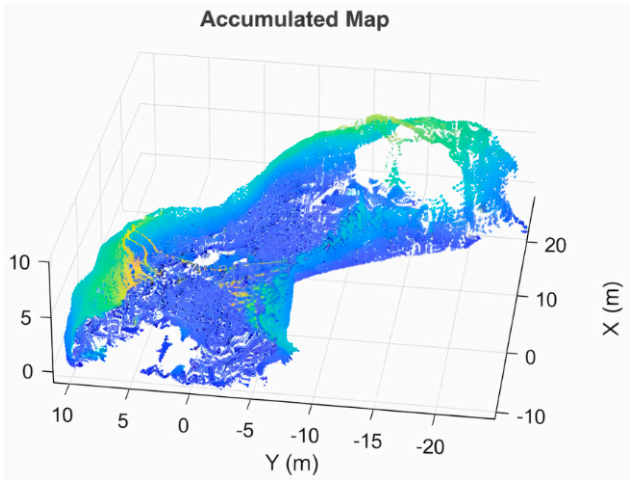

Figure 9. ICP generated map.

The comparison between ICP and ICP + IMU in Figures 7 and 8 indicates that, for the nearly rectilinear and low-dynamic trajectory considered here, inertial aiding does not provide a measurable improvement over pure ICP. In this scenario, the geometric constraints and scan overlap appear sufficient to ensure stable convergence, making the inertial prior largely redundant. However, this finding should be interpreted as scenario-dependent: IMU information is expected to become more beneficial under faster motion, with stronger

rotations and reduced overlap, or locally degenerate geometry, where it can improve initialization and mitigate convergence failures. Further experiments with more complex trajectories are therefore required to fully characterize the impact of IMU aiding in registration-based mapping pipelines.

Table 3 compares the performance of the LOAM and ICP algorithms, both with and without IMU fusion. All tests were performed on a laptop equipped with an Intel Core i7 (10th generation) processor and 16 GB of RAM. The reported computation times correspond to the average of multiple runs, in order to mitigate the natural variability of execution times. This analysis allows a comparison between the different algorithms, while actual computation time will be evaluated when the hardware equipping the rover is selected.

Table 3. Key metrics for LOAM algorithms.

Method	Computation Time [s]	RMSE [m]	Drift [m/m]
LOAM + IMU	0.1326	0.5230	0.02638
LOAM	0.1205	0.6029	0.03041
ICP + IMU	0.0485	0.4238	0.02137
ICP	0.0399	0.4239	0.02138

It is worth noting that orientation RMSE was not computed, as the rover followed a predominantly straight-line trajectory, making rotational errors not relevant for this evaluation. Drift is computed as the position RMSE divided by path length to quantify relative error accumulation.

The ICP algorithm achieved the best accuracy with a position RMSE of approximately 0.424 m and the lowest drift of about 0.0214 m/m. The integration of IMU data provided a noticeable improvement for LOAM, reducing its RMSE from 0.603 m to 0.523 m, while offering only marginal gains for the ICP.

From a computational perspective, ICP proved to be significantly faster—roughly three times quicker than LOAM—with average execution times around 0.04 s compared to 0.12–0.13 s for LOAM. As expected, the addition of IMU fusion introduces a small computational overhead in both algorithms.

The comparative evaluation of LOAM and ICP yields a consistent system-level outcome: in a lava tube context—where operation must be illumination-independent and the geometry can be weakly informative (smooth walls, low feature density, and terrain-induced height variations)—a LiDAR-only solution can generally reconstruct the planar trajectory reliably, but it tends to be less robust in full 6-DoF pose estimation, especially in terms of vertical consistency and drift susceptibility.

Adding an IMU provides complementary motion constraints that improve odometry stability and convergence when LiDAR observability degrades, thus offering a measurable robustness margin that emerges consistently across both analyses. In the feature-based case (LOAM), inertial aiding is particularly beneficial in mitigating drift and stabilizing the estimate, while in the registration-based case (ICP), IMU integration does not degrade performance; however, incorporating inertial priors remains a reasonable design choice to improve initialization and robustness in more dynamic trajectories or in locally degenerate geometric conditions.

Therefore, LiDAR + IMU is the most reliable baseline configuration for lava tube navigation, whereas LiDAR-only remains a viable fallback when system complexity must be minimized, at the cost of reduced robustness in the most challenging conditions. At the same time, a LiDAR-only layout can provide an emergency solution in the case of a failure of the IMU.

6. Proposed GNC Architecture for Lava Tubes

Autonomous operation within lava tubes requires a dedicated GNC architecture in which navigation, mapping, and decision-making are executed entirely onboard, with minimal reliance on external support.

Since communication may be available only intermittently (typically near the entrance), the system must sustain robust real-time state estimation and local trajectory generation during sustained autonomy. This motivates a LiDAR–inertial navigation backbone, complemented by wheel odometry for aiding and consistency, and coupled with energy-aware planning to ensure that exploration depth remains compatible with a guaranteed return-to-base capability.

The proposed subsurface GNC architecture includes the following elements:

- Mast (2-DOF, 800 mm height)

  The rover is equipped with an 800 mm mast carrying the LiDAR at its top. The mast provides two degrees of freedom, enabling controlled rotations about the vertical axis (yaw) and a horizontal axis (pitch).

- Solid-state LiDAR

  A 40° FOV solid-state LiDAR is selected as the primary perception sensor to generate real-time 3D point clouds, enabling navigation in total darkness. The baseline sourcing strategy targets Teledyne solutions, leveraging supplier heritage in space-qualified LiDAR systems to maximize robustness and reliability in harsh environments.

- IMU

  The inertial core is the LN-200S of Northrop Grumman, mounted as close as possible to the rover's center of mass to minimize rotational error propagation and improve inertial accuracy. The LN-200S is characterized by extensive flight heritage, including deep-space missions and Mars rover applications (e.g., Spirit, Opportunity, Curiosity, and Perseverance), making it a suitable candidate for long-duration autonomous operation in GPS-denied conditions.

- Encoder route (wheel odometry)

  Wheel encoders provide distance-traveled measurements for odometric estimation. This odometry supports multi-sensor fusion with LiDAR and IMU, improving short-term localization consistency and providing a useful redundancy channel in case of partial LiDAR degradation (e.g., dust, occlusions, and poor overlap).

- OBC (onboard computer).

  A dedicated or integrated OBC performs real-time processing for: sensor acquisition and synchronization, LiDAR–Inertial and wheel-odometry fusion, SLAM map updates, and guidance, motion planning, and control execution.

- Communication antenna and entrance relay

  A fixed relay antenna is deployed at the lava tube entrance. The rover can offload data and/or receive commands when it returns within link range, ensuring a minimal but dependable communication capability in an otherwise isolated environment.

- Battery-state monitoring for energy-aware autonomy

  Continuous, real-time monitoring of battery state is a primary input to the navigation logic. Battery data directly gates exploration depth by enabling the rover to decide when to proceed deeper and when to initiate a return-to-base maneuver, ensuring safe mission closure without external recovery options.

7. Navigation Framework Inside the Lava Tube

Operationally, upon entering the lava tube, the rover performs an initial 360° LiDAR scan to establish a first local map and geometric reference; during this phase, the LiDAR is commanded at 0° pitch relative to the ground to optimize wall intersection and delineate tunnel boundaries.

Once the lava tube entrance is identified, the rover autonomously navigates toward it. During traversal, the LiDAR is reoriented to an inclination of 30 degrees relative to the horizontal plane. This configuration enhances the perception of terrain irregularities and local elevation changes, contributing to accurate ground modeling. The two setups are shown in Figures 10 and 11, where the dashed lines and arrows indicate the two different scanning directions adopted by the sensor.

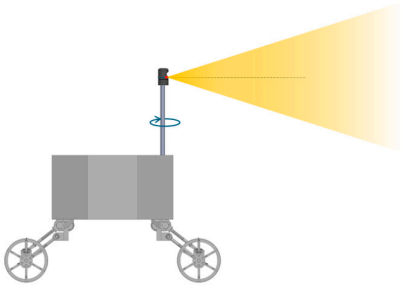

Figure 10. Rover in boundary-detection mode.

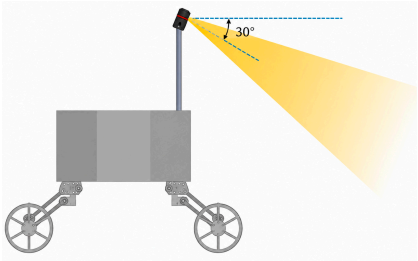

Figure 11. Rover in features-detection mode.

Throughout the mission, the SLAM subsystem continuously integrates the incoming LiDAR data (aided by IMU and odometry) to maintain an updated local map and a consistent pose estimate. Obstacles, non-traversable regions, and steep slopes are detected in real time; when hazards are identified, the system triggers local replanning to generate a safe trajectory that respects mobility constraints while continuing coverage expansion (e.g., via frontier-based target selection in unknown regions).

As the rover proceeds deeper into the lava tube, energy management becomes a critical factor for mission success. To ensure that sufficient battery capacity is preserved for a safe return, the rover evaluates its progression based on an energy constraint:

$$m \cdot g \cdot \Delta h + R \cdot s + k \cdot \Delta t \cdot c_1 \leq SOC \cdot c_{max} \cdot c_s \quad (1)$$

where:

- Δh is the cumulative descent in elevation, proportional to the energy required for the return ascent;
- R is the rolling resistance factor;
- s is the total traveled distance;
- $k \cdot \Delta t$ models the energy consumed by auxiliary systems over time, while $c_1 > 1$ introduces a safety factor to estimate the return time conservatively.

On the right-hand side:

- SOC (state of charge), c_{max} (maximum battery capacity), and $c_s < 1$ (a safety coefficient) define the effective usable energy reserve.

The rolling resistance term R can be evaluated as a function of rover mass, gravity, and terrain properties, with coefficients derived from terramechanics models or experimental campaigns on lunar regolith simulants [30,31]. Slope effects are accounted for through the gravitational term ($mg\Delta h$).

The auxiliary consumption term k can be obtained from subsystem-level power budgets, including sensing, control, and thermal control loads, as commonly performed in robotic system design and energy-aware formulations for planetary rovers [32,33].

The safety factor $c_1 > 1$ is introduced as a conservative engineering margin to account for uncertainties in return-path estimation, slip variability, path tortuosity, and local traversability. Although more advanced risk-aware approaches exist [34,35], the present work adopts a simpler margin-based strategy that can be calibrated through simulation campaigns and sensitivity analyses.

The coefficient $c_s < 1$ limits the usable battery capacity to respect recommended depth-of-discharge thresholds and to compensate for capacity fade over the mission lifetime. This conservative derating is preferred in the present preliminary design phase over more complex strategies involving real-time state-of-health monitoring and prediction [36–38].

By continuously evaluating this inequality, the rover autonomously determines whether continuing exploration is viable or whether it must begin its return journey to avoid the risk of power depletion. This energy-aware planning is especially vital in the enclosed and unstructured environment of the lava tube, where external recovery options are nonexistent and communication delays may be significant.

Figure 12 presents the main flowchart representing the navigation logic inside the lava tube.

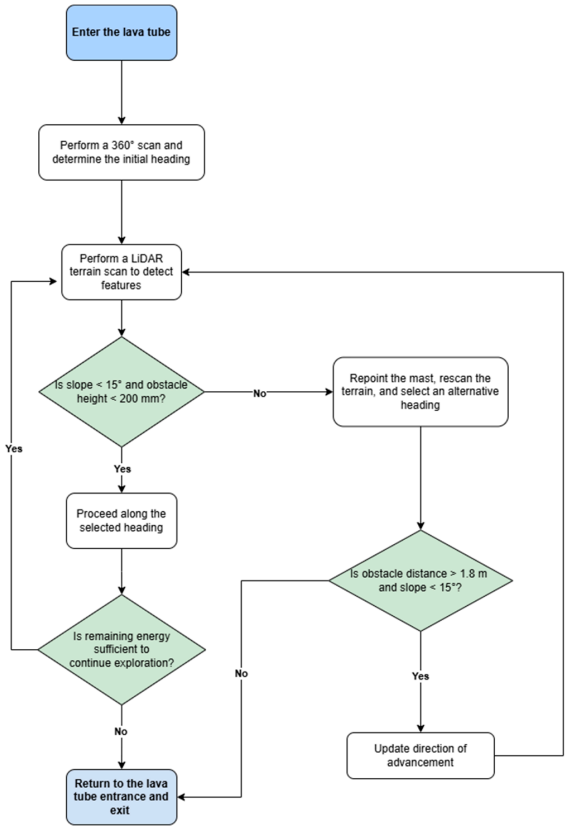

Figure 12. Flowchart of the navigation logic inside the lava tube.

8. Conclusions

This work addressed the problem of autonomous navigation in lunar lava tubes, a challenging environment characterized by the absence of illumination, limited prior knowledge of geometry, uneven terrain, and intermittent communications. A mission-oriented approach is adopted to define a suitable Guidance, Navigation, and Control (GNC) architecture capable of supporting fully autonomous operations.

A weighted-criteria evaluation framework is developed to assess different SLAM solutions under realistic mission constraints, including robustness, energy consumption, and system complexity. The analysis highlights the limitations of vision-based approaches in subsurface conditions and identifies LiDAR-based solutions as the most suitable option for reliable navigation.

The simulation campaign confirms that LiDAR-only SLAM ensures accurate planar localization but exhibits reduced robustness in full 6-DoF estimation, particularly in the vertical component and in geometrically weak scenarios. The integration of inertial measurements provides complementary motion information, improving convergence and reducing drift, thus supporting the selection of LiDAR–Inertial SLAM as the baseline configuration.

It is important to clarify that the objective of this work is to support a mission-oriented sensor selection process. ICP and LOAM are chosen as representative and well-established algorithms to quantify the benefit of adding inertial measurements to a LiDAR-based pipeline under lava-tube-like conditions.

Based on these results, a modular GNC architecture is proposed, integrating multi-sensor fusion, real-time mapping, and energy-aware navigation. This approach enables the rover to operate autonomously while ensuring safe exploration and return capabilities in the absence of continuous ground support.

Overall, the study provides a coherent methodological and architectural foundation for the design of robotic systems dedicated to lunar subsurface exploration, with potential applicability to other planetary environments.

Future work includes the selection of the most appropriate LiDAR-Inertial SLAM algorithm and the evaluation of parameters in Equation (1). Both these activities require a more detailed definition of the rover, which will become available at a more advanced phase of the design of the mission.

Author Contributions: Conceptualization: G.C., M.M., L.S., C.M.C., F.S.F., I.P., T.M. and S.M.; methodology: G.C., M.M., L.S., I.P., T.M. and S.M.; investigation: G.C., M.M., L.S. and S.M.; validation: M.M., L.S., F.S.F., T.M. and S.M.; formal analysis: A.C., L.S. and S.M.; software: A.C. and M.M.; data curation: A.C. and M.M.; resources: S.M., I.P. and C.M.C.; writing—original draft: G.C.; writing—review an editing: G.C. and S.M.; supervision: C.M.C. and S.M.; funding acquisition: C.M.C., I.P. and S.M.; project administration: C.M.C., S.M. and F.S.F. All authors have read and agreed to the published version of the manuscript.

Funding: This work was carried out under "Contratto ASI n. 2024-26-I.0" as subcontractor of OHB Italia.

Data Availability Statement: The original contributions presented in this study are included in the article. Further inquiries can be directed to the corresponding author.

Conflicts of Interest: Author Cuono Massimo Crispo, Author Francesco Saverio Fulginiti, Author Isacco Pretto, and Author Tharek Mohtar are employed by Company OHB Italia S.p.A. The authors declare that the research was conducted in the absence of any commercial or financial relationships that could be construed as a potential conflict of interest.

References

1. Feng, Y.; Pan, P.-Z.; Tang, X.; Wang, Z.; Li, Y.; Hussain, A. A comprehensive review of lunar lava tube base construction and field research on a potential Earth test site. *Int. J. Min. Sci. Technol.* **2024**, *34*, 1201–1216. [CrossRef]
2. Lin, Y.; Yang, W.; Zhang, H.; Hui, H.; Hu, S.; Xiao, L.; Liu, J.; Xiao, Z.; Yue, Z.; Zhang, J.; et al. Return to the Moon: New perspectives on lunar exploration. *Sci. Bull.* **2024**, *69*, 2136–2148. [CrossRef]
3. Ding, J.; Xie, G.; Guo, L.; Xiong, X.; Han, Y.; Wang, X. Karst Cave as Terrestrial Simulation Platform to Test and Design Human Base in Lunar Lava Tube. *Space Sci. Technol.* **2022**, *2022*, 9875780. [CrossRef]
4. Vasavada, A.R.; Bandfield, J.L.; Greenhagen, B.T.; Hayne, P.O.; Siegler, M.A.; Williams, J.; Paige, D.A. Lunar equatorial surface temperatures and regolith properties from the Diviner Lunar Radiometer Experiment. *J. Geophys. Res. Plan.* **2012**, *117*, E00H18. [CrossRef]
5. Horányi, M.; Szalay, J.R.; Wang, X. The lunar dust environment: Concerns for Moon-based astronomy. *Philos. Trans. R. Soc. A Math. Phys. Eng. Sci.* **2024**, *382*, 20230075. [CrossRef]
6. Kauahikaua, J.; Cashman, K.V.; Mattox, T.N.; Heliker, C.C.; Hon, K.A.; Mangan, M.T.; Thornber, C.R. Observations on basaltic lava streams in tubes from Kilauea Volcano, island of Hawai'i. *J. Geophys. Res. Solid Earth* **1998**, *103*, 27303–27323. [CrossRef]
7. Melchiorre, M.; Colamartino, T.; Ferrauto, M.; Troise, M.; Salamina, L.; Mauro, S. Design of a Spherical Rover Driven by Pendulum and Control Moment Gyroscope for Planetary Exploration. *Robotics* **2024**, *13*, 87. [CrossRef]
8. Melchiorre, M.; Salamina, L.; Mauro, S.; Pastorelli, S. Design of a Spherical UGV for Space Exploration. In *IAC, 2022*; International Astronautical Federation (IAF): Paris, France, 2022.
9. Lee, S.-B.; Cho, N.; Lee, G.; Lee, S.; Kim, J.; Shim, G.; Jang, J.T.; Kim, S.K.; Seo, T.; Sim, C.K.; et al. Soft deployable airless wheel for lunar lava tube intact exploration. *Sci. Robot.* **2025**, *10*, eadx2549. [CrossRef]
10. Ye, J.; Lab, V. The Realizing of Autonomous Navigation in Lunar Rover Virtual Simulation System. *Mach. Des. Res.* **2009**. Available online: https://www.semanticscholar.org/paper/The-Realizing-of-Autonomous-Navigation-in-Lunar-Ye-Lab/f6efec56391ba39ca53e9d3a444de87b332eab51 (accessed on 24 May 2026).
11. Wang, Y.; Zhang, W.; An, P. A survey of simultaneous localization and mapping on unstructured lunar complex environment. In Proceedings of the 2nd International Conference on Materials Science, Resource and Environmental Engineering (MSREE 2017), Wuhan, China, 27–29 October 2017; p. 030010. [CrossRef]
12. Cadena, C.; Carlone, L.; Carrillo, H.; Latif, Y.; Scaramuzza, D.; Neira, J.; Reid, I.; Leonard, J.J. Past, Present, and Future of Simultaneous Localization and Mapping: Toward the Robust-Perception Age. *IEEE Trans. Robot.* **2016**, *32*, 1309–1332. [CrossRef]
13. Melchiorre, M.; Salamina, L.; Scimmi, L.S.; Mauro, S.; Pastorelli, S. Experiments on the Artificial Potential Field with Local Attractors for Mobile Robot Navigation. *Robotics* **2023**, *12*, 81. [CrossRef]
14. Salamina, L.; Gaidano, M.; Melchiorre, M.; Mauro, S. Mobile Robot With Robotic Arm: Development and Validation of a Digital Twin. In *Volume 3: Advanced Manufacturing*; American Society of Mechanical Engineers: New York City, NY, USA, 2023; Volume 3. [CrossRef]
15. Rohmer, E.; Singh, S.P.N.; Freese, M. V-REP: A versatile and scalable robot simulation framework. In *2013 IEEE/RSJ International Conference on Intelligent Robots and Systems*; IEEE: New York City, NY, USA, 2013; pp. 1321–1326. [CrossRef]
16. She, X.; Wang, J.; Xu, W.; Xiao, L. Research on the impact of extraterrestrial lava tube environments on human survival and countermeasures. *Space Habitat.* **2025**, *1*, 100002. [CrossRef]
17. Kalita, H.; Thangavelautham, J. Strategies for Deploying a Sensor Network to Explore Planetary Lava Tubes. *Sensors* **2021**, *21*, 6203. [CrossRef]
18. Naito, M.; Hasebe, N.; Shikishima, M.; Amano, Y.; Haruyama, J.; Matias-Lopes, J.A.; Kim, K.J.; Kodaira, S. Radiation dose and its protection in the Moon from galactic cosmic rays and solar energetic particles: At the lunar surface and in a lava tube. *J. Radiol. Prot.* **2020**, *40*, 947–961. [CrossRef]
19. Blair, D.M.; Chappaz, L.; Sood, R.; Milbury, C.; Bobet, A.; Melosh, H.J.; Howell, K.C.; Freed, A.M. The structural stability of lunar lava tubes. *Icarus* **2017**, *282*, 47–55. [CrossRef]
20. Ebadi, K.; Chang, Y.; Palieri, M.; Stephens, A.; Hatteland, A.; Heiden, E.; Thakur, A.; Funabiki, N.; Morrell, B.; Wood, S.; et al. LAMP: Large-Scale Autonomous Mapping and Positioning for Exploration of Perceptually-Degraded Subterranean Environments. In *2020 IEEE International Conference on Robotics and Automation (ICRA)*; IEEE: New York City, NY, USA, 2020; pp. 80–86. [CrossRef]
21. Sahili, A.R.; Hassan, S.; Sakhrieh, S.M.; Mounsef, J.; Maalouf, N.; Arain, B.; Taha, T. A Survey of Visual SLAM Methods. *IEEE Access* **2023**, *11*, 139643–139677. [CrossRef]
22. Jinyu, L.; Bangbang, Y.; Danpeng, C.; Nan, W.; Guofeng, Z.; Hujun, B. Survey and evaluation of monocular visual-inertial SLAM algorithms for augmented reality. *Virtual Real. Intell. Hardw.* **2019**, *1*, 386–410. [CrossRef]
23. Hong, S.; Bangunharcana, A.; Park, J.-M.; Choi, M.; Shin, H.-S. Visual SLAM-Based Robotic Mapping Method for Planetary Construction. *Sensors* **2021**, *21*, 7715. [CrossRef]
24. Huang, L. Review on LiDAR-based SLAM Techniques. In *2021 International Conference on Signal Processing and Machine Learning (CONF-SPML)*; IEEE: New York City, NY, USA, 2021; pp. 163–168. [CrossRef]

25. Zhang, J.; Singh, S. LOAM: Lidar Odometry and Mapping in Real-time. In *Robotics: Science and Systems X*; Robotics: Science and Systems Foundation: Los Angeles, CA, USA, 2014. [CrossRef]
26. Chen, J.; Wang, H.; Yang, S. Tightly Coupled LiDAR-Inertial Odometry and Mapping for Underground Environments. *Sensors* **2023**, *23*, 6834. [CrossRef]
27. Shan, T.; Englot, B.; Meyers, D.; Wang, W.; Ratti, C.; Rus, D. LIO-SAM: Tightly-coupled Lidar Inertial Odometry via Smoothing and Mapping. In *2020 IEEE/RSJ International Conference on Intelligent Robots and Systems (IROS)*; IEEE: New York City, NY, USA, 2020; pp. 5135–5142. [CrossRef]
28. Available online: https://ti.arc.nasa.gov/dataset/caves/ (accessed on 12 February 2025).
29. Besl, P.J.; McKay, N.D. A method for registration of 3-D shapes. *IEEE Trans. Pattern Anal. Mach. Intell.* **1992**, *14*, 239–256. [CrossRef]
30. Ishigami, G.; Miwa, A.; Nagatani, K.; Yoshida, K. Terramechanics-based model for steering maneuver of planetary exploration rovers on loose soil. *J. Field Robot.* **2007**, *24*, 233–250. [CrossRef]
31. Jiang, M.; Dai, Y.; Cui, L.; Xi, B. Experimental and DEM analyses on wheel-soil interaction. *J. Terramech.* **2018**, *76*, 15–28. [CrossRef]
32. Hou, L.; Zhang, L.; Kim, J. Energy Modeling and Power Measurement for Mobile Robots. *Energies* **2018**, *12*, 27. [CrossRef]
33. Sakayori, G.; Ishigami, G. Energy-aware trajectory planning for planetary rovers. *Adv. Robot.* **2021**, *35*, 1302–1316. [CrossRef]
34. Ono, M.; Fuchs, T.J.; Steffy, A.; Maimone, M.; Yen, J. Risk-aware planetary rover operation: Autonomous terrain classification and path planning. In *2015 IEEE Aerospace Conference*; IEEE: New York City, NY, USA, 2015; pp. 1–10. [CrossRef]
35. Sánchez-Ibáñez, J.R.; Sanchez-Cuevas, P.J.; Olivares-Mendez, M. Optimal and Risk-Aware Path Planning considering Localization Uncertainty for Space Exploration Rovers. In *2022 IEEE/RSJ International Conference on Intelligent Robots and Systems (IROS)*; IEEE: New York City, NY, USA, 2022; pp. 4092–4099. [CrossRef]
36. Salinas-Camus, M.; Kulkarni, C.; Orchard, M. Battery State-of-Health Aware Path Planning for a Mars Rover. In Proceedings of the Annual Conference of the PHM Society, Salt Lake City, UT, USA, 28 October–2 November 2023; Volume 15. [CrossRef]
37. Zhang, B.; Tang, L.; DeCastro, J.; Roemer, M.; Goebel, K. Autonomous Vehicle Battery State-of-Charge Prognostics Enhanced Mission Planning. *Int. J. Progn. Health Manag.* **2014**, *5*. [CrossRef]
38. Daigle, M.; Kulkarni, C.S. A battery health monitoring framework for planetary rovers. In *2014 IEEE Aerospace Conference*; IEEE: New York City, NY, USA, 2014; pp. 1–9. [CrossRef]